

Model-driven CT reconstruction algorithm for nano-resolution x-ray phase contrast imaging

Yuhang Tan(谭雨航), Xuebao Cai(蔡学宝), Jiecheng Yang(杨杰成), Ting Su(苏婷), Hairong Zheng(郑海荣), Dong Liang(梁栋), Peiping Zhu(朱佩平), and Yongshuai Ge(葛永帅)

Citation: Chin. Phys. B, 2024, 33 (**7**): 078702. DOI: 10.1088/1674-1056/ad3dcc
Journal homepage: http://cpb.iphy.ac.cn; http://iopscience.iop.org/cpb

What follows is a list of articles you may be interested in

Investigations of moiré artifacts induced by flux fluctuations in x-ray dark-field imaging

Zhi-Li Wang(王志立), Zi-Han Chen(陈子涵), Yao Gu(顾瑶), Heng Chen(陈恒), and Xin Ge(葛昕)
Chin. Phys. B, 2023, 32 (**3**): 038704. DOI: 10.1088/1674-1056/ac946a

Super-resolution reconstruction algorithm for terahertz imaging below diffraction limit

Ying Wang(王莹), Feng Qi(祁峰), Zi-Xu Zhang(张子旭), and Jin-Kuan Wang(汪晋宽)
Chin. Phys. B, 2023, 32 (**3**): 038702. DOI: 10.1088/1674-1056/aca9c7

Modeling hydrogen exchange of proteins by a multiscale method

Wentao Zhu(祝文涛), Wenfei Li(李文飞), and Wei Wang(王炜)
Chin. Phys. B, 2021, 30 (**7**): 078701. DOI: 10.1088/1674-1056/abe377

A modified interval subdividing based geometric calibration method for interior tomography

Zhang Feng (张峰), Yan Bin (闫镔), Li Lei (李磊), Xi Xiao-Qi (席晓琦), Jiang Hua (江桦)
Chin. Phys. B, 2014, 23 (**9**): 098704. DOI: 10.1088/1674-1056/23/9/098704

Image reconstruction based on total-variation minimization and alternating direction method in linear scan computed tomography

Zhang Han-Ming (张瀚铭), Wang Lin-Yuan (王林元), Yan Bin (闫镔), Li Lei (李磊), Xi Xiao-Qi (席晓琦), Lu Li-Zhong (陆利忠)
Chin. Phys. B, 2013, 22 (**7**): 078701. DOI: 10.1088/1674-1056/22/7/078701

Model-driven CT reconstruction algorithm for nano-resolution x-ray phase contrast imaging

Yuhang Tan(谭雨航)[1], Xuebao Cai(蔡学宝)[2], Jiecheng Yang(杨杰成)[1], Ting Su(苏婷)[1], Hairong Zheng(郑海荣)[1,3], Dong Liang(梁栋)[1,3], Peiping Zhu(朱佩平)[4], and Yongshuai Ge(葛永帅)[1,3,†]

[1] *Research Center for Medical Artificial Intelligence, Shenzhen Institute of Advanced Technology, Chinese Academy of Sciences, Shenzhen* 518055, *China*
[2] *Institute of Electronic Paper Displays, South China Academy of Advanced Optoelectronics, South China Normal University, Guangzhou* 510006, *China*
[3] *Paul C Lauterbur Research Center for Biomedical Imaging, Shenzhen Institute of Advanced Technology, Chinese Academy of Sciences, Shenzhen* 518055, *China*
[4] *Institute of High Energy Physics, Chinese Academy of Sciences, Beijing* 100049, *China*

(Received 24 January 2024; revised manuscript received 29 March 2024; accepted manuscript online 12 April 2024)

The low-density imaging performance of a zone plate-based nano-resolution hard x-ray computed tomography (CT) system can be significantly improved by incorporating a grating-based Lau interferometer. Due to the diffraction, however, the acquired nano-resolution phase signal may suffer splitting problem, which impedes the direct reconstruction of phase contrast CT (nPCT) images. To overcome, a new model-driven nPCT image reconstruction algorithm is developed in this study. In it, the diffraction procedure is mathematically modeled into a matrix $\boldsymbol{B}$, from which the projections without signal splitting can be generated invertedly. Furthermore, a penalized weighted least-square model with total variation (PWLS-TV) is employed to denoise these projections, from which nPCT images with high accuracy are directly reconstructed. Numerical experiments demonstrate that this new algorithm is able to work with phase projections having any splitting distances. Moreover, results also reveal that nPCT images of higher signal-to-noise-ratio (SNR) could be reconstructed from projections having larger splitting distances. In summary, a novel model-driven nPCT image reconstruction algorithm with high accuracy and robustness is verified for the Lau interferometer-based hard x-ray nano-resolution phase contrast imaging.

Keywords: splitting phase image, reconstruction algorithm, grating interferometer

PACS: 87.59.–e, 07.85.Tt, 07.60.Ly, 42.30.Rx **DOI:** 10.1088/1674-1056/ad3dcc

1. Introduction

The x-ray CT imaging with nano-resolution is a powerful technique in detecting the three-dimensional (3D) ultra-fine structures inside the object.[1] For low-density objects, however, conventional x-ray imaging may not be able to provide sufficient image contrast due to the subtle variations of the absorption coefficients between two different materials. To overcome such difficulty, the grating-based x-ray Lau interferometer was coupled with the zone plate hard x-ray CT imaging system.[2–4] By doing so, the phase information that carries better image contrast can be retrieved. When a Lau interferometer is incorporated into an nPCT imaging system,[2–4] however, both theory and experiments show that strong signal splitting would appear due to the dramatically magnified x-ray beam diffraction by the zone plate.[3,5] Clearly, such signal splitting would hinder the direct reconstructions of nPCT images[6] from the acquired projections.

To overcome, Takano *et al.* proposed an image deconvolution-based nPCT reconstruction algorithm.[6] In it, the phase signal recovery is achieved through a combination of signal post-processing procedures such as deconvolution and Fourier transformation. By doing so, projections without signal splitting can be obtained to allow the following reconstructions of nPCT images. To mitigate the potential discontinuous phase artifacts,[7] Ueda *et al.* recently proposed a three-wave interference model to iteratively reconstruct the nPCT images from the measured beam intensities. In this study, a model-driven nPCT image reconstruction algorithm is proposed. In particular, the beam diffraction is mathematically expressed by an operator $\boldsymbol{B}$, from which the projections without signal splitting are recovered inversely. Additionally, a penalized weighted least-square model[8] with total variation (PWLS-TV) is employed to perform image denoising. Finally, nPCT images are reconstructed via the filtered back projection (FBP) algorithm.

2. Signal model

In the following discussions, it is assumed that the nPCT imaging system comprises an x-ray source (integrated with a condenser), an object, a zone plate, a $\pi/2$ phase grating, and a detector, see the illustration in Fig. 1. Note that the zone plate is used to magnify the image of the object, and the $\pi/2$ phase grating is used to encode the phase information of the x-ray beam. Assuming the complex refractive index of the object is denoted as $n(x) = 1 - \delta(x) + \mathrm{i}\beta(x)$, thus, the extracted phase signal Φ is expressed as[3,5]

†Corresponding author. E-mail: ys.ge@siat.ac.cn

© 2024 Chinese Physical Society and IOP Publishing Ltd

$$\Phi(x) = \varphi\left(x+\frac{\Delta s}{2}\right) - \varphi\left(x-\frac{\Delta s}{2}\right), \tag{1}$$

where

$$\varphi(x) = k\int \delta(x)\,\mathrm{d}z \tag{2}$$

denotes the phase signal before splitting, $\Delta s = 2\lambda d/p$ denotes the diffraction induced splitting distance, k and λ represent the wave number and wavelength, respectively, d denotes the distance between phase grating and detector, and p is the period of phase grating. Be aware that the phase signal Φ is an opposite-superposition $(-)$ of the paired diffraction signals φ in Eq. (1). Due to the non-zero splitting Δs, as a consequence, the phase signal Φ cannot be directly utilized to reconstruct nPCT images.

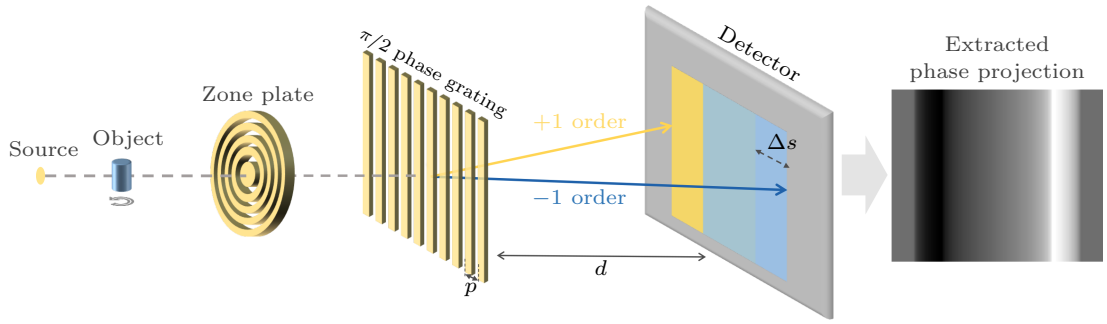


Fig. 1. Illustration of a hard x-ray nano-resolution computed tomography (CT) system integrated with a zone plate and a Lau interferometer. The x-ray beam diffracts and splits on the $\pi/2$ phase grating, resulting in signal overlapping for the extracted phase contrast projection. Herein, the ±1 diffraction orders are annotated for the $\pi/2$ phase grating.

3. Reconstruction algorithm

Mathematically, the signal diffraction, *i.e.*, signal splitting, can be expressed by a matrix $\boldsymbol{B}$. With it, the phase projection Φ in Eq. (1) can be rewritten as

$$\Phi = \boldsymbol{B}\varphi + n_\varphi, \tag{3}$$

where n_φ represents the signal noise. According to Eq. (1), matrix $\boldsymbol{B}$ is defined as

$$\boldsymbol{B} = \boldsymbol{b}_{m\times m} + \boldsymbol{O}, \tag{4}$$

where

$$\boldsymbol{b}_{m\times m} = \begin{bmatrix} 0 & \cdots & 0 & -1_{i,i+\Delta}^{i\le\Delta} & 0 & \cdots & \cdots & 0 \\ \vdots & \vdots & \vdots & \vdots & \ddots & \vdots & \vdots & \vdots \\ 0 & \cdots & 1_{i,i-\Delta}^{\Delta<i\le m-\Delta} & \cdots & \cdots & -1_{i,i+\Delta}^{\Delta<i\le m-\Delta} & \cdots & 0 \\ \vdots & \vdots & \vdots & \ddots & \vdots & \vdots & \vdots & \vdots \\ 0 & \cdots & \cdots & 0 & 1_{i,i-\Delta}^{i>m-\Delta} & 0 & \cdots & 0 \end{bmatrix}, \tag{5}$$

matrix $\boldsymbol{O} = \mathrm{diag}(\gamma,\gamma,\ldots,\gamma)$ $(\gamma = 10^{-12})$ guarantees the invertibility of $\boldsymbol{B}$, index m refers to the number of detector elements, $\Delta = \Delta s/(2w)$ denotes the splitting of half of signal separation in terms of the number of detector elements with width w, i and j represent the indices of row and column in the matrix, respectively. The work flow of $\boldsymbol{B}$ is illustrated in Fig. 2. If ignoring signal noise n_φ, essentially, the phase signal φ in Eq. (3) without splitting can be solved by $\boldsymbol{B}^{-1}\Phi$, see Fig. 2.

The analytical inversion of Eq. (3) would dramatically magnify the image noise. To mitigate, the penalized weighted least-square model with total variation (PWLS-TV) is applied. As demonstrated, the PWLS-TV algorithm can effectively enhance the image quality, i.e., signal-to-noise-ratio (SNR), while preserving the edges and details.[8] In the case of nPCT imaging, the objective function is formulated as[8]

$$\varphi^* = \arg\min_{\varphi\ge0}\left\{(\Phi-\boldsymbol{B}\varphi)^{\mathrm{T}}\Lambda^{-1}(\Phi-\boldsymbol{B}\varphi) + \alpha\boldsymbol{R}_{\mathrm{TV}}(\varphi)\right\}, \tag{6}$$

where $\alpha = 0.02$ denotes a smoothing parameter that controls the consistency between the estimation and measurement, Λ denotes a diagonal matrix with the q^{th} detector element $\sigma_{\varphi_q}^2$ equals to[9]

$$\sigma_{\varphi_q}^2 = \frac{2}{\varepsilon^2\sum_{k=1}^{M} I_q^{(k)}}. \tag{7}$$

Herein, ε represents the response efficiency of the interferometer and was set to 0.5 in this study, M denotes the total number of phase steps, and I_q represents the detected photons in the q^{th} detector element. In Eq. (6), the prior term $\boldsymbol{R}_{\mathrm{TV}}(\varphi)$ is defined

as

$$\boldsymbol{R}_{\mathrm{TV}}(\varphi)=\sum_{q}\sqrt{\left(\varphi_{q}-\varphi_{q-1}\right)^{2}+\upsilon}, \tag{8}$$

where υ is a small constant used for keeping $\boldsymbol{R}_{\mathrm{TV}}(\varphi)$ differentiable with respect to image intensity.

The gradient descent method is used to iteratively solve the above optimization problem. Particularly,

$$\begin{aligned}\varphi^{t} &= \varphi^{(t-1)}-\eta^{(t-1)}\left(\boldsymbol{B}^{\mathrm{T}}\left(\Lambda^{-1}\left(\boldsymbol{B}\varphi^{(t-1)}-\boldsymbol{\Phi}\right)\right)\right)\\ &-\alpha\tau\frac{\nabla\boldsymbol{R}_{\mathrm{TV}}\left(\varphi^{(t-1)}\right)}{\left\|\nabla\boldsymbol{R}_{\mathrm{TV}}\left(\varphi^{(t-1)}\right)\right\|},\end{aligned} \tag{9}$$

in which φ^{t} denotes the optimized phase image obtained from the t^{th} iteration, $\nabla\boldsymbol{R}_{\mathrm{TV}}\left(\varphi^{(t-1)}\right)$ denotes the gradient of the regularizer, τ denotes a scalar factor and is fixed at 1.0, $\eta^{(t-1)}$ denotes the gradient step size[10]

$$\begin{aligned}\eta^{t-1}&=\frac{G^{\mathrm{T}}G}{(\boldsymbol{B}G)^{\mathrm{T}}(\Lambda^{-1}(\boldsymbol{B}G))}\quad\text{with}\\ G&\triangleq\boldsymbol{B}^{\mathrm{T}}\left(\Lambda^{-1}\left(\boldsymbol{B}\varphi^{t-1}-\boldsymbol{\Phi}\right)\right).\end{aligned} \tag{10}$$

By repeating the signal processing procedure in Eq. (9) for all projection views, the unsplitted and denoised sinogram $S_{\varphi^{t}}$ would be obtained, see more details in Fig. 2. By the way, the total number of iterations is fixed at 100, which is empirically is enough to provide satisfactory results with balanced noise level and image resolution.

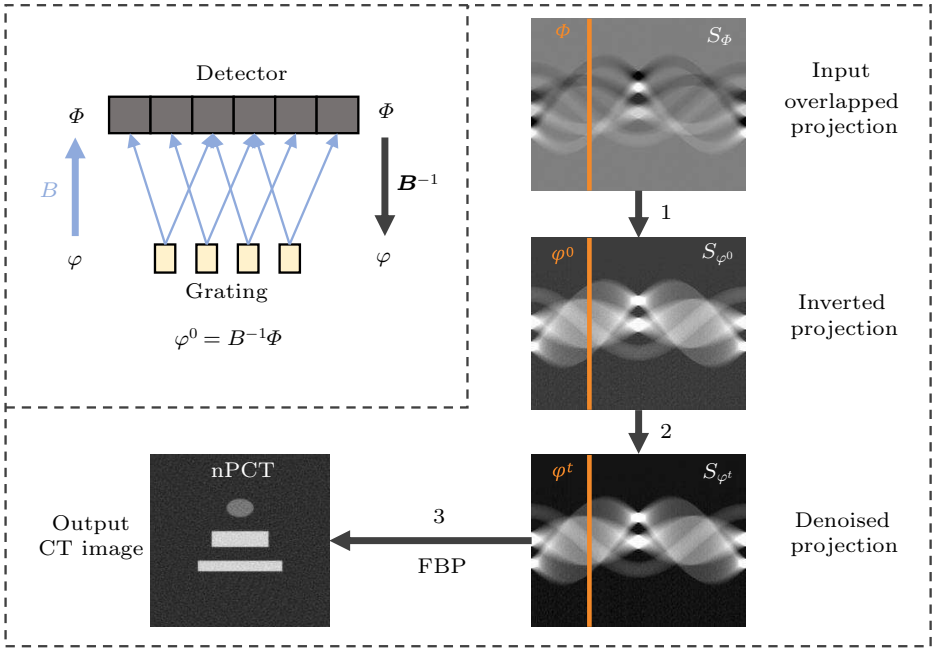


Fig. 2. Workflow of the proposed nPCT image reconstruction algorithm. In step one, the overlapped projection S_{Φ} is converted to the unsplitted projection $S_{\varphi^{0}}$ using $\boldsymbol{B}^{-1}$. In step two, image $S_{\varphi^{0}}$ is iteratively denoised according to Eq. (9) for all projection views. In the final step, nPCT images are reconstructed from $S_{\varphi^{t}}$ using the FBP algorithm. The highlighted line denotes the phase projection acquired at a certain view.

4. Numerical experiments and results

Numerical experiments were conducted to verify the proposed image reconstruction algorithm that was developed in Python (Version 3.10). First of all, a two-dimensional (2D) phantom was simulated, see Fig. 3. The numerical phantom has a size of 512×512 with pixel dimension of 10 nm. It consists three groups of circles, rings, and bars. They are made of three low-density materials: lung tissue (LT), protein and polystyrene (PS). All the numerical simulations were performed on our previously developed x-ray nPCT imaging platform.[5] In brief, the x-ray beam energy was 8.04 keV, 10000 x-ray photons were incident on the sample with Poisson noise, and the overall system magnification was 650. In total, 720 projections were captured by a 0.5 degree angular interval within a full rotation. The one-dimensional (1D) detector array has a size of 1×600, and each element has a dimension of 6.5 μm.

To compare, nPCT images were reconstructed from three different approaches. First, the acquired phase projections S_{Φ} containing signal splitting were reconstructed directly without any post-processing. Second, nPCT images were reconstructed from the analytically inverted phase signal $S_{\varphi^{0}}$ before image denoising. Third, nPCT images were reconstructed using the PWLS-TV denoised phase signal $S_{\varphi^{t}}$. Herein, the parallel CT imaging geometry was assumed, and the conventional FBP algorithm with Hilbert filter kernel for S_{Φ} and ramp filter kernel for $S_{\varphi^{0}}$ and $S_{\varphi^{t}}$ was implemented. Results are presented in Fig. 3. As seen, the direct reconstruction would lead to very blurry nPCT images. As a contrary, the inversion of phase signal would significantly enhance the image sharpness.

Moreover, the PWLS-TV approach can further reduce the image noise, see the highlighted region-of-interests (ROIs). The residual differences with respect to the numerical phantom are depicted in the bottom. On average, it takes less than a second to process one projection of size 512×512. The computation was performed on an Intel Xeon Silver 4210R CPU.

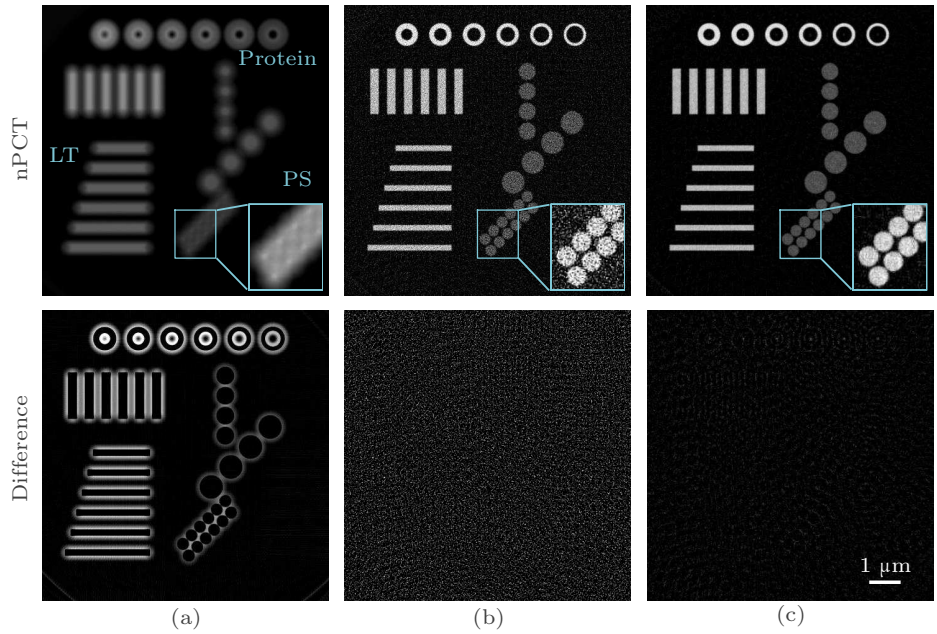


Fig. 3. Comparison results with splitting distance $\Delta s = 200$ nm. The nPCT images are reconstructed from (a) S_{Φ}, (b) S_{φ^0}, and (c) S_{φ^t}. The display window is $[0,\ 1.2 \times 10^{-5}]$. The differences between the reconstructed nPCT images and the ground truth are shown below with a display window of $[0,\ 4.5 \times 10^{-6}]$. The scale bar denotes 1 μm.

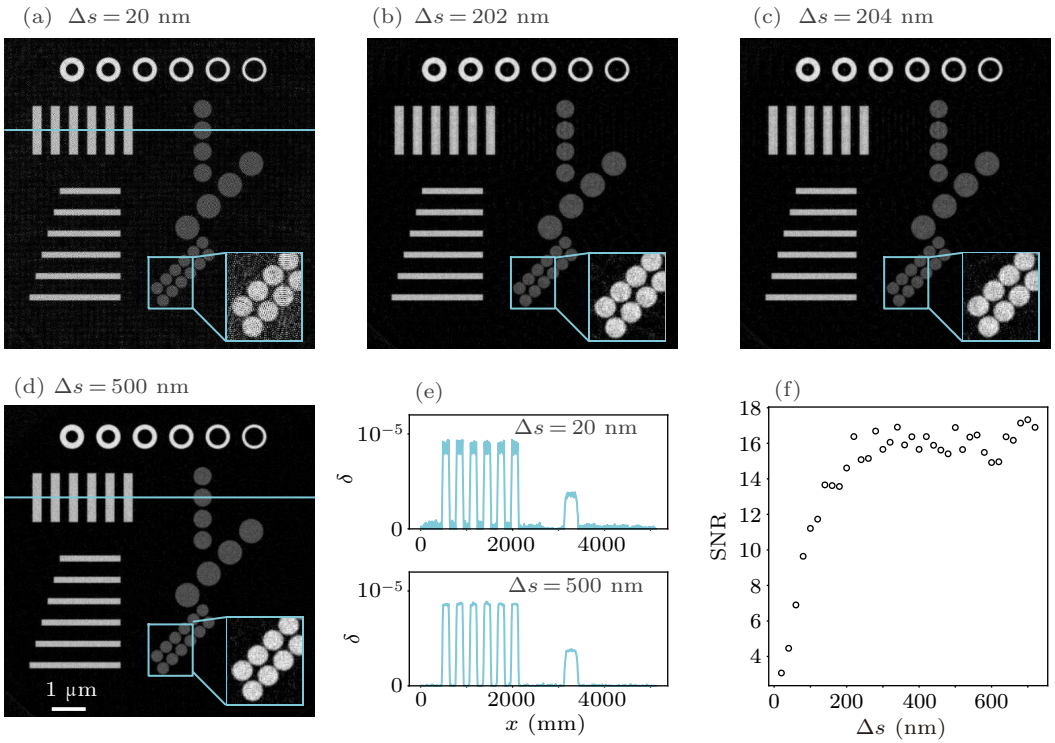


Fig. 4. Results for different separation distance Δs with pixel dimension of 10 nm. (a) $\Delta s = 20$ nm, (b) $\Delta s = 202$ nm, (c) $\Delta s = 204$ nm, (d) $\Delta s = 500$ nm. (e) The profile of highlighted line in panels (a) and (d). (f) Relationship between SNR and Δs for nPCT. The scale bar denotes as 1 μm, and the gray scales of all images are identical from 0 to 1.2×10^{-5}.

Additionally, the impact of the signal splitting Δs to the quality of the reconstructed nPCT images was also investigated quantitatively. Images in Fig. 4 display the reconstructed nPCT results at four different splitting distances: $\Delta s = 20$, 202, 204, and 500 nm. For $\Delta s = 202$ nm and $\Delta s = 204$ nm, which correspond to non-integer ($\Delta = 10.1$ and $\Delta = 10.2$) number

of detector elements, the element $b_{i,j}$ in matrix $\boldsymbol{b}_{m\times m}$ used in Eq. (4) is defined as

$$b_{i,j} = \begin{cases} f-1, & j = i+\Delta, \\ -f, & j = i+\Delta+1, \\ f, & j = i-\Delta-1, \\ 1-f, & j = i-\Delta, \\ 0, & \text{otherwise}, \end{cases} \tag{11}$$

where f corresponds to the fractional part of Δ. For instance, if $\Delta = 10.1$, then $f = 0.1$. Moreover, the relationship between image SNR and Δs is plotted as well, see Fig. 4(f). Interestingly, it is found that larger signal splitting Δs leads to nPCT images with improved SNR. As Δs gets large enough, SNR tends to become constant. It is guessed that this might be related to the noise correlation induced by the signal overlapping. As can be imagined, less signal overlapping leads to fewer solution of matrix $\boldsymbol{B}$, thus resulting in less image noise. Currently, we do not have thorough explanations to it and further investigations are needed in the future.

5. Discussion and conclusion

This study proposes a new model-based nPCT image reconstruction algorithm to overcome the signal splitting problem occurred in the nPCT imaging system coupled with a zone plate and a Lau interferometer. In it, the diffraction induced signal splitting is modeled by an operation matrix $\boldsymbol{B}$, which can be well defined and analytically inverted. As a result, the phase signal before splitting can be recovered immediately and straightforwardly. Additionally, the PWLS-TV method is developed to reduce the image noise of the recovered unsplitting phase signal. Moreover, numerical experiments are performed to validate this newly developed nPCT image reconstruction algorithm. Results demonstrate that this proposed method can ensure high-precision nano-resolution phase contrast CT imaging. Additionally, since the phase signal overlapping model for the nPCT imaging system with a π phase grating is identical with the $\pi/2$ phase grating imaging system, therefore, the reconstruction algorithm proposed in this work remains applicable.

The current study has several limitations that could be improved in the future. First, the imaging model defined in Eq. (1) is built for the extracted phase image containing signal splitting rather than for the acquired x-ray intensity signals containing diffraction fringes.[7] In the latter imaging model, the signal splitting operation $\boldsymbol{B}$ also needs to be incorporated to describe the forward imaging procedure to directly reconstruct the nPCT images. Second, the current model-based image reconstruction algorithm does not focus on the nPCT image denoising. To reduce image noise, the value of the weight α added before the regularizer in Eq. (6) needs to be adjusted properly. To this end, nPCT imaging with lower radiation dose could be obtained. Such a kind of interesting investigations would be performed with this algorithm in the future. Third, nPCT image reconstruction with splitted phase signals could be performed by the latest deep learning technique,[11] especially with the convolutional neural networks (CNN). One advancement of using CNN lies in generating better image quality with shorter processing time. However, thousands of network training images needs to be prepared in advance. From our previous experience,[12] this could be easily solved using numerical data such as the natural images downloaded from the ImageNet.[13,14] Fourth, this model-based nPCT image reconstruction algorithm assumes that the phase signals are partially overlapped. Therefore, it is not suitable to work with phase signals having no overlapping. Namely, the phase signals having splitting distance that is larger than the object dimension. When this happens, the conventional FBP algorithm along with Ramp kernel could be utilized directly to reconstruct the nPCT images.

In conclusion, a novel model-driven nano-resolution phase contrast CT image reconstruction algorithm is developed for the Lau interferometer-based nano-resolution hard x-ray phase contrast imaging. With it, high quality nPCT images can be generated for the overlapped phase signals containing arbitrary splitting distances.

Acknowledgements

Project supported by the National Natural Science Foundation of China (Grant No. 12027812) and the Guangdong Basic and Applied Basic Research Foundation of Guangdong Province, China (Grant No. 2021A1515111031).

References

[1] Momose A 2017 *Microscopy* **66** 155
[2] Takeda Y, Yashiro W, Hattori T, Takeuchi A, Suzuki Y and Momose A 2008 *Appl. Phys. Express* **1** 117002
[3] Yashiro W, Takeda Y, Takeuchi A, Suzuki Y and Momose A 2009 *Phys. Rev. Lett.* **103** 180801
[4] Yashiro W, Harasse S, Takeuchi A, Suzuki Y and Momose A 2010 *Phys. Rev. A* **82** 043822
[5] Yang J, Zhu P, Liang D, Zheng H and Ge Y 2022 *Chin. Phys. B* **31** 098702
[6] Takano H, Hashimoto K, Nagatani Y, Irwin J, Omlor L, Kumar A, Tkachuk A, Wu Y and Momose A 2019 *Optica* **6** 1012
[7] Ueda R, Hashimoto K, Takano H, Cai M and Momose A 2021 *SPIE* **11840** 78
[8] Fessler J A 1994 *IEEE Transactions on Medical Imaging* **13** 290
[9] Chen G, Zambelli J, Li K, Bevins N and Qi Z 2011 *Med. Phys.* **38** 584
[10] Kawata, S and Nalcioglu O 1985 *IEEE Transactions on Medical Imaging* **4** 65
[11] Zhou B, Shi B, Jin D and Liu X 2015 *Nat. Nanotechnol.* **10** 924
[12] Ge Y, Su T, Zhu J, Deng X, Zhang Q, Chen J, Hu Z, Zheng H and Liang D 2020 *Quant. Imaging Medicine Surg.* **10** 415
[13] Su T, Sun X, Yang J, Mi D, Zhang Y, Wu H, Fang S, Chen Y, Zheng H and Liang D 2022 *Med. Phys.* **49** 917
[14] Zhu J, Su T, Zhang X, Yang J, Mi D, Zhang Y, Gao X, Zheng H, Liang D and Ge Y 2022 *Phys. Medicine & Biol.* **67** 145012